JOURNAL OF APPLIED ELECTROCHEMISTRY 22 (1992) 285–292

Investigations on N-halogen cyclic ureide based magnesium primary cell system at various temperatures

R. UDHAYAN, D. P. BHATT*, P. B. MATHUR

Laboratories of the Batteries and Fuel Cell Division, Central Electrochemical Research Institute, Karaikudi 623 006, India

Received 16 January 1991; revised 29 April 1991

This paper reports the results of experimental studies on a magnesium/magnesium perchlorate/N,N′-dichlorodimethylhydantoin cell system at various temperatures ranging from 70 to −20° C. A constant current discharge method was employed to evaluate the battery parameters such as discharge capacity, energy density, coulombic efficiency and internal resistance. Cyclic voltammetric (CV) investigations of the N,N′-dichlorodimethylhydantoin (DDH) were carried out in 0.1 M magnesium perchlorate medium in order to supplement the results. Scanning electron microscopy (SEM) was performed on post-polarized magnesium samples to follow the morphological changes in the anodic material with respect to temperatures. These investigations broadly reveal that the cell system can give rise to the open-circuit/closed-circuit voltage of $\gtrsim 2.0$ V and it is possible to obtain current densities of 20 mA cm^{-2} during discharge.

1. Introduction

In recent years there has been a world-wide interest in research and development of magnesium-organic battery systems [1–4]. A series of organic compounds based on nitro, nitroso and peroxy type functional groups has been explored [5, 6]. The magnesium/meta-dinitrobenzene system has received much attention as a promising primary cell due to its multi-electron transfer property during electrochemical reduction [7, 8]. This nitro compound has, however, a low cathodic potential and, hence, when it is coupled with a magnesium anode the cell shows a voltage of 1.05–1.10 V at a 50 h discharge rate [9]. Halogens, on the other hand, have long been considered as attractive materials for their use as cathodes in battery devices because of their high electrode potential and high specific capacity. There have been several attempts to utilize these materials in electrochemical power sources [10, 11], but so far the problems of corrosion or the handling associated with these elements has not been overcome. In an effort to circumvent these problems, we have undertaken a study of the N,N′-dichlorodimethylhydantoin (DDH) based magnesium cell system. Previous reports are available on the preliminary investigation on the Zn/DDH system [12].

Since magnesium possesses a higher electrode potential (−2.37 V for Mg; −0.76 V for Zn), a lower electrochemical equivalent (0.45 g Ah^{-1} for Mg; 1.22 g Ah^{-1} for Zn) and an excellent shelf-life, it has, therefore, prompted the authors to couple magnesium with a DDH organic cathode to form a higher energy density cell system in comparison to the Zn/DDH system. Although magnesium has an edge over zinc in respect of the above parameters, it suffers from the disadvantage of a higher self corrosion rate. Two types of reaction generally take place in magnesium cells during discharge:

(i) useful electrochemical current-producing reaction

$$Mg + 2OH^- \longrightarrow Mg(OH_2) + 2e^- \quad (1)$$

(ii) wasteful corrosion reaction

$$Mg + 2H_2O \longrightarrow Mg(OH)_2 + H_2 \quad (2)$$

Reaction 2 occurs during discharge as well as in idle conditions of the cell, which in turn results in the reduction of the overall material efficiency of the magnesium anode. To some extent, Reaction 2 can be controlled by selecting an appropriate electrolyte. Magnesium perchlorate has been found to be an ideal electrolyte for this purpose in comparison with other, well-known, electrolytes such as magnesium chloride and magnesium bromide. Also the complete control of Reaction 2 is neither possible nor warranted due to the fact that passive film formation of $Mg(OH)_2$ on the surface of magnesium is an inherent characteristic which is responsible for enhancing the shelf-life in magnesium cells. This wasteful self-corrosion reaction again becomes advantageous at high altitudes due to the generation of a considerable amount of heat (172 kJ eq^{-1} of magnesium) within the cell system.

In view of these facts, further research was conducted on this novel Mg/DDH system over a wide temperature range between +70 and −20 °C. The discharge characteristics of Mg/DDH cells was studied at various currents, *viz.* 10 to 250 mA. Cyclic voltammetric behaviour of DDH on a platinum electrode at different temperatures was also investigated. Scanning

* To whom correspondence should be addressed.

0021-891X/92

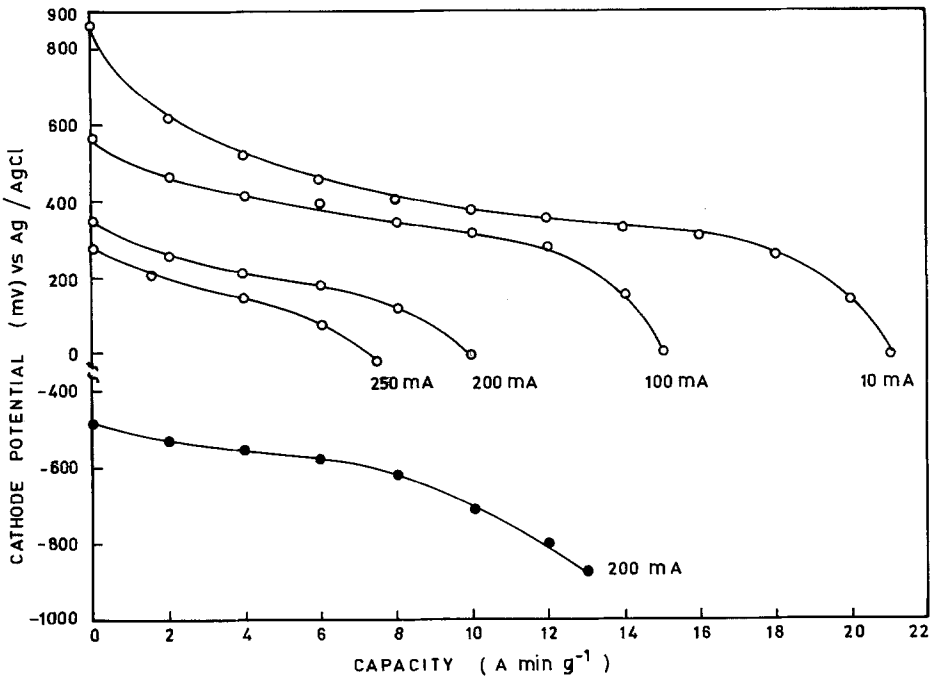

Fig. 1. Half-cell potential measurements of DDH (○) and metadinitrobenzene (●) cathodic depolarizers.

electron microscopy (SEM) has been employed to characterize the morphology of the post-polarized magnesium electrode at each temperature.

2. Experimental details

2.1. *Cell fabrication and discharge measurements*

AZ 31 magnesium alloy (composition: Al 2.5–3.5%, Zn 0.6–1.4% and Mn 0.15–0.70%) sheets were obtained from Magnesium Elektron Ltd, UK. The anode sheets of dimensions: 2 cm × 3 cm × 0.5 cm were used in the experiments. The top portion of the magnesium anode was soldered to a copper wire for electrical connection. The titanium expanded grid (6 mesh) of the same size as that of magnesium anode was used as the current collector for the cathode. The cathode mix containing 1 g DDH (Aldrich), 0.5 g acetylene black (Travancore Chemicals (India), commercial pure grade) and 0.5 to 1.0 ml of an aq. solution of 2% carboxymethylcellulose (BDH) binder was spread over the titanium mesh at an optimized pressure employing a hydraulic press (Peeco Oil-Hydraulic Equipment Co.). Mg/DDH cells were fabricated using two anodes and one cathode which were separated by special synthetic paper. The Inter-electrode distance was about 2 mm. A 2.0 M magnesium perchlorate (Baker AR grade) electrolyte solution was used to activate the cell. Before the commencement of the discharge experiment, the cells were left idle in the electrolyte for sufficient time to enable the active materials of the system to attain the desired temperature and steady state open circuit voltage (o.c.v.). Voltage against time characteristics of the cells were measured at constant currents of 10, 25, 50, 75, 100, 125, 150, 200 and 250 mA. The tests were conducted at −20, −10, 0, 10, 20, 30, 50 and 70 ± 1 °C in different sets of experiments. Another set of experiments was performed in order to describe the *i–E* relationship at each temperature. The waiting period between current increments was 30 s. Capacities of Mg/DDH cells were calculated against the cut-off voltage of 1.5 V. Triplicate experiments were performed and the reproducibility was ±2%.

2.2. *Half-cell potential measurements*

In these experiments, an Ag/AgCl reference electrode (3.0 M NaCl) was connected to the organic cathode and the half-cell potentials of DDH and meta-dinitrobenzene (*m*-DNB) were measured as a function of time during discharge at a constant temperature of 30 ± 1 °C. The method of preparation of the *m*-DNB cathode was as in the case of DDH. Capacity was calculated by multiplying the discharge time and current drain. For comparison, the difference of the initial and cut-off potential was kept the same in both DDH and *m*-DNB cathodes.

2.3. *Cyclic voltammetry measurements*

An aq. 0.1 M magnesium perchlorate solution containing 1.9608 mM DDH (prepared in 100% ethanol) was used for the cyclic voltammetry (CV) experiments. All the solutions were prepared in double distilled water.

CV measurements were carried out with a BAS-100A Electrochemical Analyser (West Lafayette, Indiana, USA) and the *i–E* profiles were plotted on a digital plotter (DMF-40 series, Houston Instrument Division). The electrochemical cell consisted of a platinum working electrode (0.0314 cm^2) embedded in Teflon,® a Ag/AgCl reference electrode and a platinum foil auxiliary electrode. The platinum working electrode was pretreated electrochemically in a similar manner as reported elsewhere [13]. CV profiles were recorded between the potential limits of −200 and −600 mV employing various scan rates (5, 10, 20, 40, 100, 200

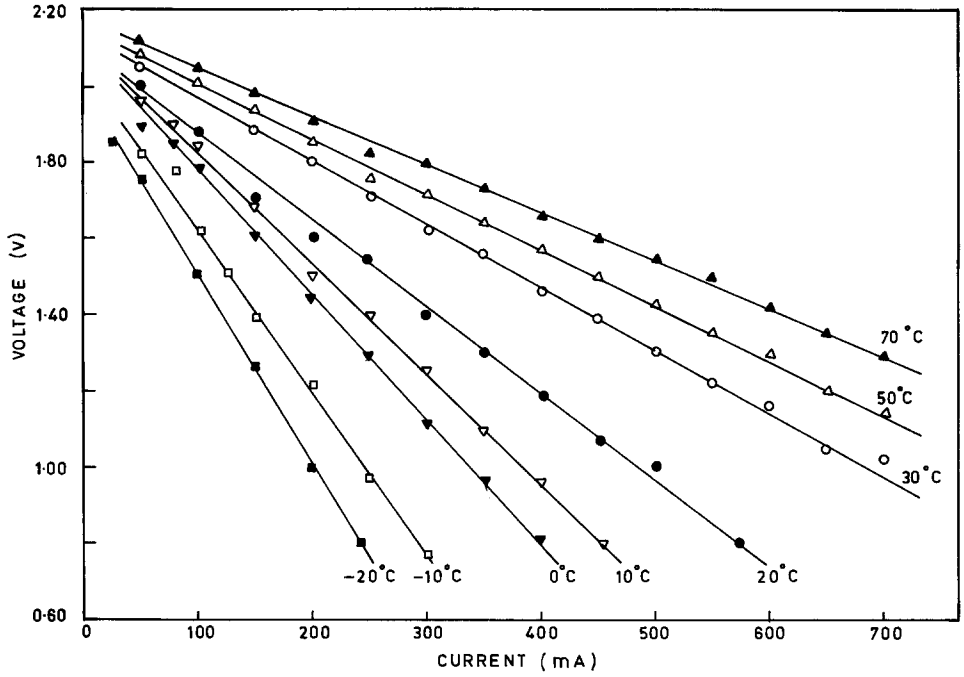

Fig. 2. Voltage against current drain curves of Mg/DDH cell at different temperatures.

and 300 mV s^{-1}) and temperatures (0, 30, 40, 50 and 60°C). Purified nitrogen was bubbled to the electrolytic cell before each set of measurements. All the potentials were referred to the Ag/AgCl electrode (E = 0.210 V/NHE).

2.4. *SEM measurements*

Immediately after attaining the cut-off voltage of the discharged cell, the magnesium sheets were cleaned in a boiling solution of 20% chromic acid and 0.02% silver nitrate [14] followed by washing with double distilled water. After drying, the samples were transferred to the SEM unit (JEOL, JSM-35 CF, Japan make) for analysis.

3. Results and discussion

The current and voltage developed in the present electrochemical primary energy system is governed by the reaction of magnesium metal (anode) with the organic cathode. The reduction of DDH proceeds by taking up the hydroxyl ions from the aq. magnesium perchlorate electrolyte. This reaction does not occur in the absence of reactive metals like zinc [12] and magnesium. The individual electrochemical reactions can be represented as follows:

Anodic reaction

$$2Mg \longrightarrow 2Mg^{2+} + 4e^-$$

Cathodic reaction

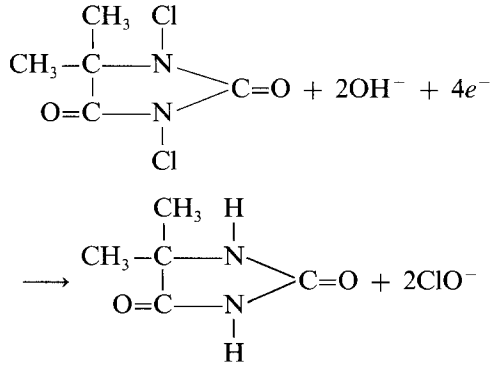

3.1. *Cathode potential against cell capacity measurements*

Figure 1 shows the half-cell potential of the DDH

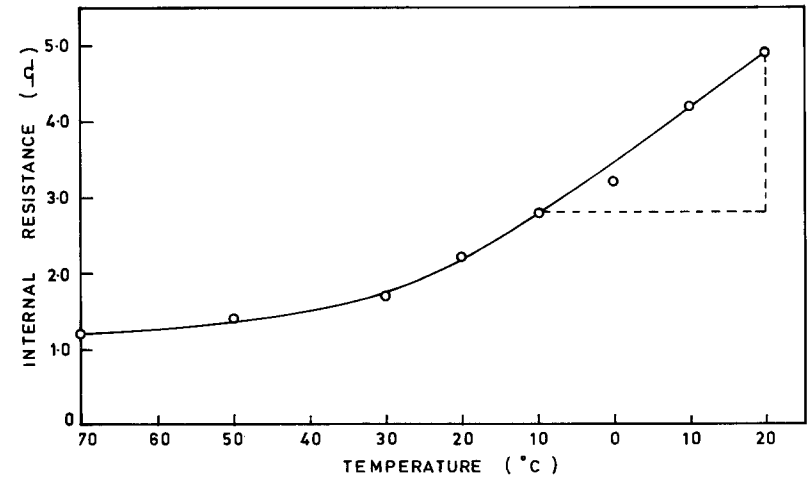

Fig. 3. Dependence of internal resistance of Mg/DDH cell with temperature.

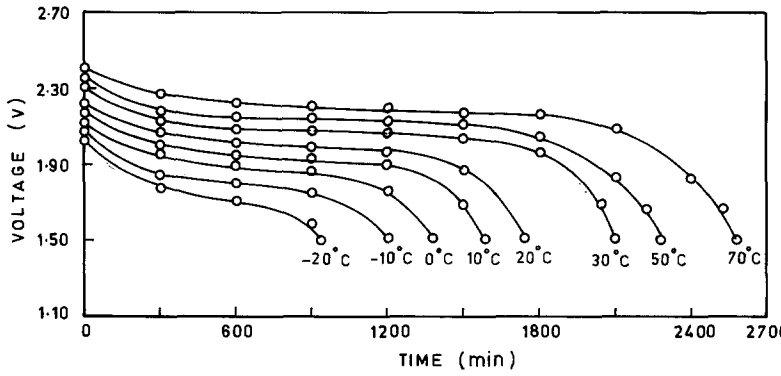

Fig. 4. Voltage against time curves of Mg/DDH cell at different temperatures (current drain: 10 mA).

cathode against the cell capacity at various currents. A comparison of the present system with *m*-DNB is also shown under identical conditions at a constant current of 200 mA. The difference of the initial and cut-off potential of the two cathodic systems is kept the same for the sake of comparison. It may be noted from Fig. 1 that the cut-off cathodic potentials of DDH and *m*-DNB are O mV and −900 mV, respectively. The corresponding cut-off voltages of the Mg/DDH and Mg/*m*-DNB cell systems are observed to be 1.5 and 0.5 V, respectively. It should be noted that the cell capacity shown in the figure for *m*-DNB based cell system is not the real capacity. The real capacity of the Mg/*m*-DNB cell was found to be 17 Ah (kg of *m*-DNB)$^{-1}$ at the nominal cut-off voltage of 0.75–0.80 V, the corresponding cut-off potential of the *m*-DNB cathode was −515 mV, as is evident from the figure. It is, therefore, imperative that the *m*-DNB based cell system is not discharged at higher currents. Further experiments at the higher current of 250 mA gave rise to negligibly small discharge duration. This indicates the limitation of the *m*-DNB cathode for higher rate applications [9]. These experiments suggest that a workable current density of 20 mA cm^{-2} (contact area of the electrode: 12 cm^2) can be obtained from the DDH cell system without adversely affecting the performance of the cell. The o.c.p. of *m*-DNB is 0.12 V whereas for the DDH cathode it is ~1.0 V, which is significantly higher. The figure indicates that the closed circuit potentials (c.c.p.) of DDH when discharged at various currents of 10, 100, 200 and 250 mA are 870, 570, 350 and 280 mV, respectively. These potential values are 2.5 times greater than that of *m*-DNB (−580 mV) irrespective of the current drain. The higher cathodic potential of DDH may be attributed to the attachment of loosely bonded halogen (electron attracting group) to the ring of the cyclic ureide.

3.2. *Voltage against current measurements*

The voltage and current drain results at various temperatures are shown in Fig. 2. The linear behaviour of the Mg/DDH cell at each temperature is indicative of the fact that the polarization is ohmic controlled. It can also be seen that the cell polarization gradually increases with decrease of temperature from 70 to −20 °C. It is interesting to note that the cell gives rise to current drains of 1085, 925 and 800 mA at 70, 50 and 30 °C, respectively, at the end of discharge. Decreasing the temperature to 20, 10, 0, −10 and −20 °C results in a further current decrease in the order of 570, 453, 400, 290 and 240 mA, respectively. This shows that the discharge of the cell system at lower temperatures (−20 °C) produces greater polarization due to the higher internal resistance, which arises because of the poor conductivity of the electrolyte at sub-zero temperatures. A plot of internal resistance against temperature is shown in Fig. 3. This curve indicates that the internal resistance does not vary much between 30 and 70 °C and for this range of temperature, the slope of the curve (i.e. the temperature coefficient: dR/dT) is almost constant and is calculated to be 0.007 mΩ °C^{-1}. However, there is a pronounced change in the internal resistance when the temperature region is between 30 to 10°C for which the slope is found to be 0.053 mΩ °C^{-1}. Likewise, from 10 to −20 °C, the slope is 0.07 mΩ °C^{-1}. This dR/dT data may enable a prediction of the fall in the voltage for a particular cell design provided the temperatures and current ranges are well specified.

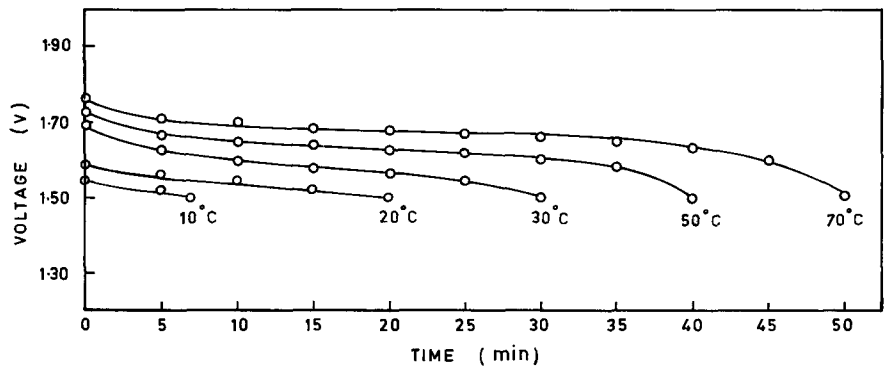

Fig. 5. Voltage against time curves of Mg/DDH cell at different temperatures (current drain: 250 mA).

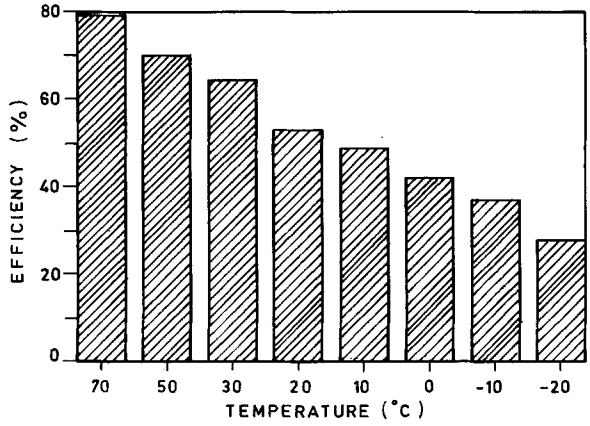

Fig. 6. Experimental histogram of Mg/DDH cell showing the dependence of efficiency with temperatures (current drain: 10 mA).

3.3. *Voltage against time measurements*

The discharge of Mg/DDH cells was carried out galvanostatically under continuous operating conditions at various current drains. Although data are available in the paper for all current drains, the discharge characteristics are shown only for two extreme current drains, *viz.* 10 and 250 mA (Figs 4 and 5). The flat plateau working voltage of the cells at different temperatures are given in parentheses, i.e. 70 °C (2.20 V), 50 °C (2.12 V), 30 °C (2.06 V), 20 °C (1.98 V), 10 °C (1.92 V), 0 °C (1.86 V), −10 °C (1.80 V) and −20 °C (1.70 V). It is clear from Fig. 4 that the lowering of temperature results in the gradual decrease in cell capacity. The cell discharge capacities i.e. Ah (kg of DDH)$^{-1}$ are calculated at each temperature and the corresponding values are shown in parentheses as: 70 °C (430), 50 °C (380), 30 °C (350), 20 °C (290), 10 °C (265), 0 °C (230), −10 °C (200) and −20 °C (155). Figure 5 illustrates a similar type of experiment by employing the highest current drain of 250 mA at different temperatures. The flat plateau voltage in this range of 10 to 70 °C is observed in between 1.54 and 1.68 V. The discharge capacities of the cell at 70, 50, 30, 20 and 10 °C are 208, 167, 125, 83 and 30 Ah (kg of DDH)$^{-1}$, respectively. From these values, the energy density was calculated. The practical coulombic efficiency of the cell was also determined under various conditions of discharge on the basis of Faraday's law (four electron transfer reaction is assumed for the calculation). These parameters are presented in Tables 1 and 2. These tables reveal that an increase of current drain from 10 to 250 mA result in a gradual loss in capacity, e.g., the specific capacity became 52% at 70 °C, 56% at 50 °C, 64% at 30 °C, 71% at 20 °C and 89% at 10 °C. The trend in the relationship between energy density and current drain and temperature is similar to the case of the discharge capacity values. However, we find that in contrast to the other well-known organic systems like *m*-DNB, where the energy density is usually lower than the corresponding discharge capacity, the present Mg/DDH system performs better in terms of higher energy density due to its higher operating voltage. It can also be seen from Tables 1 and 2 that a decrease of temperature from 70 to −20 °C causes a gradual loss in the coulombic efficiency of the cell at each current drain. The percentage loss in the coulombic efficiency (%) is given in parentheses: 10 mA (65), 25 mA (66), 50 mA (77) and 75 mA (89).

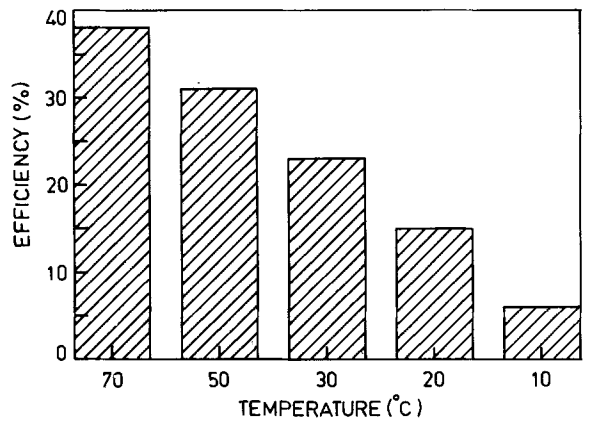

Fig. 7. Experimental histogram of Mg/DDH cell showing the dependence of efficiency with temperatures (current drain: 250 mA).

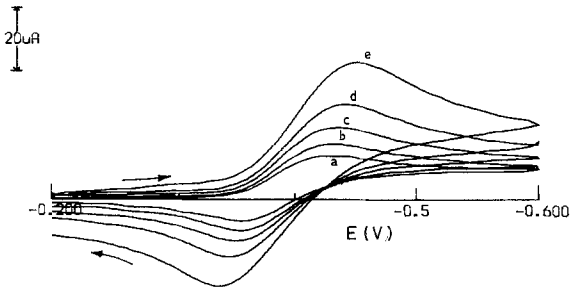

Fig. 8. CV profiles of DDH (1.9608 mM) in 0.1 M $Mg(ClO_4)_2$ medium using platinum working electrode at 0 °C and at various scan rates (a) 5, (b) 10, (c) 20, (d) 40 and (e) 100 mV s^{-1}.

Typical bar diagrams of coulombic efficiency and temperature are illustrated in Figs 6 and 7. At a constant current drain of 10 mA, the fall in coulombic efficiency for various temperatures of 70, 50, 30, 20, 10, 0, −10 and −20 °C are 11, 19, 33, 38, 47, 53 and 65%, respectively. At the highest current drain of 250 mA, similar parameters observed at 50, 30, 20 and 10 °C are 18, 39, 61 and 84, respectively. This shows

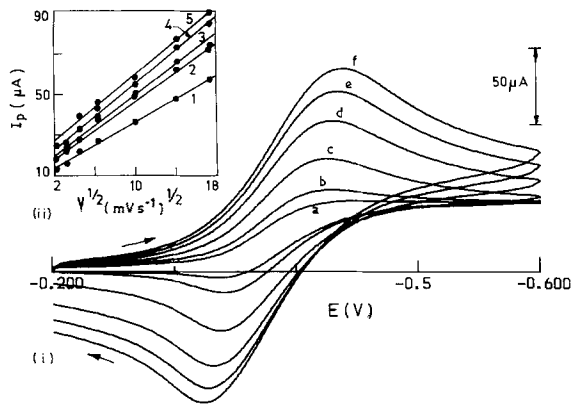

Fig. 9. (i) CV profiles of DDH (1.9608 mM) in 0.1 M $Mg(ClO_4)_2$ medium using platinum working electrode at 60 °C and at various scan rates (a) 20, (b) 40, (c) 100, (d) 200, (e) 300 and (f) 400 mV s^{-1}. (ii) Linear plots of cathodic peak current and square root of scan rate for 1.9608 mM DDH at various temperatures (1) 0, (2) 30, (3) 40, (4) 50 and (5) 60 °C.

Table 1. Discharge capacity, energy density and coulombic efficiency data of Mg/DDH cells at different current drains.

Temp.	10 mA			25 mA			50 mA			75 mA			100 mA		
(°C)	A	B	C	A	B	C	A	B	C	A	B	C	A	B	C
70	430	838	79	363	670	67	338	612	62	332	592	61	317	560	58
50	380	732	70	338	617	62	313	562	58	300	532	55	283	497	52
30	350	665	64	300	540	55	292	518	54	275	482	51	250	437	46
20	290	538	53	257	462	47	225	393	41	200	342	37	175	295	32
10	265	487	49	238	425	44	188	325	34	168	287	31	117	195	21
0	230	415	42	200	355	37	150	255	28	113	188	21	83	137	15
−10	200	357	37	168	297	31	117	193	21	75	123	14	25	38	5
−20	155	272	28	125	210	23	75	122	14	38	60	7	–	–	–

A: Ah (kg of DDH)$^{-1}$; B: Wh (kg of DDH)$^{-1}$; C: efficiency (%).

Table 2. Discharge capacity, energy density and coulombic efficiency data of Mg/DDH cells at different current drains.

Temp.	125 mA			150 mA			200 mA			250 mA		
(°C)	A	B	C	A	B	C	A	B	C	A	B	C
70	292	513	54	275	478	51	250	425	46	208	340	38
50	260	453	48	250	432	46	200	337	37	167	270	31
30	230	398	42	213	365	39	167	275	31	125	200	23
20	147	240	27	125	200	23	100	155	18	83	128	15
10	93	152	17	50	80	9	40	62	7	30	45	6
0	63	100	11	38	60	7	–	–	–	–	–	–

A: Ah (kg of DDH)$^{-1}$; B: Wh (kg of DDH)$^{-1}$; C: efficiency (%).

that the cell performs with greater efficiency at low current drains and higher temperatures.

3.4. *Cyclic voltammetry of DDH at various temperatures*

Prior to the addition of DDH to the cell, cyclic voltammograms were recorded using the blank electrolyte of 0.1 M $Mg(ClO_4)_2$ on a platinum electrode. No peaks were observed in $Mg(ClO_4)_2$ which shows that the blank electrolyte is neither oxidized nor reduced in the potential range employed. However, on addition of DDH to the electrolyte, well-defined cathodic and anodic peaks were observed (Figs 8 and 9). This redox behaviour can be described by the following reaction scheme:

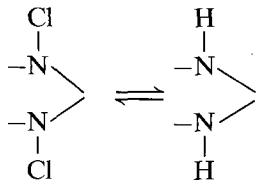

*Table 3. Peak potential and peak current data of 1.9608 mM DDH at various temperatures.**

Temperature (°C)	E_{pc} (mV)	I_{pc} (μA)	E_{pa} (mV)	I_{pa} (μA)	ΔE_p (mV)
0	−453	36	−338	37	115
30	−442	49	−349	55	93
40	−436	50	−347	56	89
50	−430	55	−342	61	88
60	−428	58	−340	72	88

* Scan rate: 100 mV s^{-1}.

CV's were recorded using 1.9608 mM DDH in a supporting medium of 0.1 M $Mg(ClO_4)_2$ at different temperatures, *viz.* 0, 30, 40, 50 and 60 °C. Typical voltammograms are shown at 0 and 60 °C (Figs 8 and 9). Well defined single anodic and cathodic peaks were observed at scan rates of 5, 10, 20, 40 and 100 mV s^{-1}. However, the E_{pc} shifts are more cathodic on increasing the scan rate, the reverse being true for the reverse sweep. This results in a large shift in peak potentials and, as is evident from Fig. 8, the increase of scan rate from 5 to 100 mV s^{-1} (at 0 °C) changes the ΔE_p from 74 to 115 mV. Variation of temperature from zero to 60 °C (Fig. 9) results in a gradual decrease of peak separation, ΔE_p (Table 3). These values are higher than that expected for a $4e^-$ transfer reaction process which indicate that the system is not completely reversible in $Mg(ClO_4)_2$ medium. The CVs also indicate that the peak current, I_p increases gradually with increase in the scan rate. Linear plots of I_p against the square root of scan rate are shown in Fig. 9(ii) at different

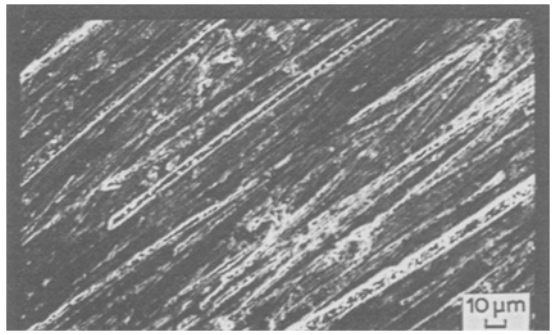

Fig. 10. SEM micrograph of pre-polarized magnesium alloy (AZ 31) (X 500).

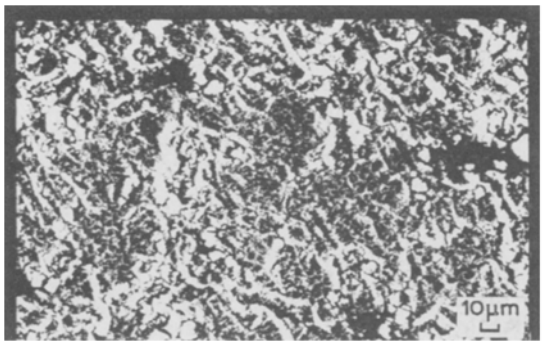

Fig. 11. SEM micrograph of post-polarized magnesium alloy at −20 °C (X 500).

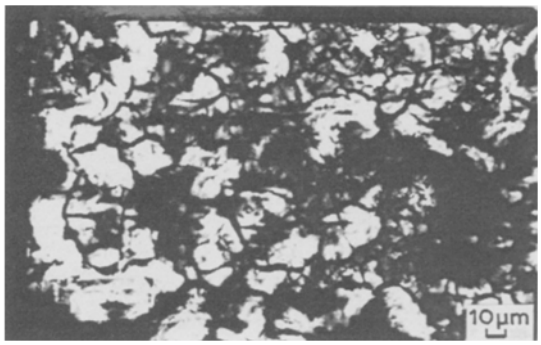

Fig. 13. SEM micrograph of post-polarized magnesium alloy at 10 °C (X 500).

temperatures. The straight lines do not pass through the origin which shows that the electrochemical redox behaviour results from both diffusion and kinetic control. Table 3 indicates that as the temperature decreases from 60 to 0 °C, I_p decreases gradually and E_{pc} shifts more cathodic values. This is the reason for observing a higher capacity at higher temperatures. These studies confirm previously reported discharge data.

3.5. *Interpretation of SEM results*

The micrograph (Fig. 10) shows a more or less uniform segregated pattern indicative of the presence of a multiphase system *viz.*, $Mg–Al_x–Zn_y$. Figures 11 to 15 show post-polarized magnesium samples discharged at a constant current of 25 mA at temperatures ranging from −20 to +70 °C. At −20°C, it appears as if grains and boundaries are covered with a film (Fig. 11) which is very resistive. Grain boundaries are slightly corroded and clearly visible at 0 °C (Fig. 12) and also the film is irregularly developed at this temperature. Further increase in temperature is expected to bring about more dissolution of the metal which is noticed at 10 °C in the related micrograph (Fig. 13). In this case, accumulation of the corrosion film begins on the surface and cracks appear over the corrosion product layer, i.e. the fractality of the electrode becomes much more evident [15]. Due to the formation of these cracks, a direct path is likely to be established between the electrode and electrolyte, which may result in continued corrosion. Figures 14 and 15 are micrographs of the post-polarized magnesium surfaces at 30 and 70 °C, respectively. The corrosion product appears to have spread over the surface in a discontinuous fashion and the corrosion rate, therefore, becomes higher. At higher temperatures, this film continues to be more and more porous, non-adherent and less protective. These results are in close agreement with both the basic and applied observations.

The viability of the system for application in tropical conditions including those in India will be further explored.

4. Conclusions

These investigations show that DDH exhibits a much higher o.c.p. of 1.0 V by comparison with other well-known organic depolarizers like *m*-DNB which has an o.c.p. of 0.120 V. The c.c.p. of DDH is also found to be higher, around 900 mV at the low discharge rates. The $Mg/Mg(ClO_4)_2$/DDH cell shows a high o.c.v. of 2.5 V and a c.c.v. of 2.0–2.4 V which are higher when compared with conventional Mg/*m*-DNB system (o.c.v.: 1.45 V; c.c.v.: 0.90–1.10 V). The workable discharge rate of the cell is up to 250 mA current drain or 20 mA cm^{-2} current density. The cell capacity is maximum at lower current drains and higher temperatures. At 70 °C, the discharge capacity and the energy density of the cell at a typical discharge rate of 10 mA are reported to be 430 Ah (kg of DDH)$^{-1}$ and 838 Wh (kg of DDH)$^{-1}$, respectively. The non-toxicity of the anodic [16] and cathodic materials [17, 18] is another positive parameter for the acceptability of this novel Mg/DDH system for practical use. Studies are underway in this direction.

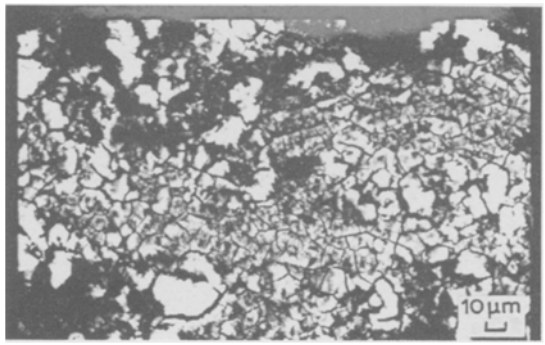

Fig. 12. SEM micrograph of post-polarized magnesium alloy at 0 °C (X 500).

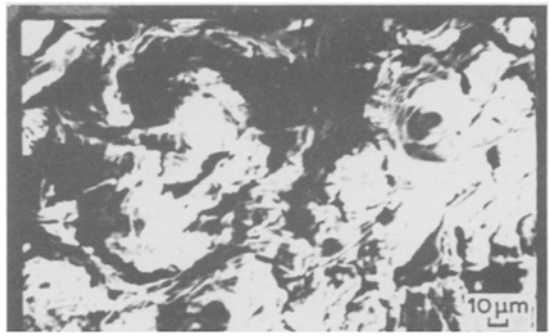

Fig. 14. SEM micrograph of post-polarized magnesium alloy at 30 °C (X 500).

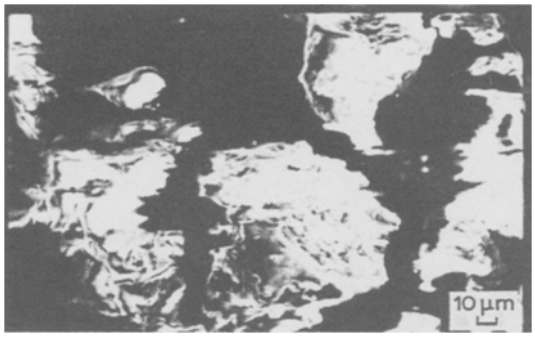

Fig. 15. SEM micrograph of post-polarized magnesium alloy at 70 °C (X 500).

Acknowledgements

The authors are indebted to Professor S. K. Rangarajan, Director of the Central Electrochemical Research Institute, Karaikudi, for his kind encouragement during this investigation and to the Council of Scientific and Industrial Research (CSIR), New Delhi, for the award of a Senior Research Fellowship to RU.

References

[1] R. Glicksman and C. K. Morehouse, *J. Electrochem. Soc.* **107** (1960) 717.
[2] E. A. McElhill, D. C. Williams and B. A. Gruber, Proceedings of the 17th Annual Power Sources Conference, Red Bank, New Jersey (1963) 145.
[3] N. T. Nicholas, Proceedings of the 21st Annual Power Sources Conference, New Jersey (1967) 113.
[4] J. C. Pawlak, 'Organic Depolarizer Primary Batteries', Technical Report ECOM-2753, Progress Report I (1976).
[5] R. Glicksman and C. K. Morehouse, *J. Electrochem. Soc.* **105** (1958) 613.
[6] K. Sivasamy, S. Rajeswary and K. Dakshinamurthi, *J. Power Sources* **25** (1989) 295.
[7] D. P. Bhatt, N. Muniyandi, R. Balasubramanian and P. B. Mathur, *Bull. Electrochem.* **2** (1986) 27.
[8] D. P. Bhatt, N. Muniyandi and P. B. Mathur, International Conference on Batteries and Fuel Cells, Karaikudi, India, Abstr. No. 43 (1988).
[9] M. A. Gutjahar and K. D. Beccu, Ext. Abstr. no. 279, Electrochem Society Meeting, Los Angeles (1970) 678.
[10] K. W. Zenger, *German Patent* 26819 (1884).
[11] P. L. Howard, *J. Electrochem. Soc.* **99** (1952) 206c.
[12] R. Udhayan, N. Muniyandi and P. B. Mathur, *J. Appl. Electrochem.*, **22** (1991) 555.
[13] P. B. Mathur, C. Srividya Rajagopalan and D. P. Bhatt, *J. Power Sources* **19** (1987) 269.
[14] F. A. Champion, 'Corrosion testing procedures', 2nd ed. Chapman and Hall, London (1964) p. 188.
[15] B. B. Mandelbrot, 'The Fractal Geometry of Nature', Freeman, San Francisco (1982).
[16] B. V. Ratnakumar and S. Sathyanarayana, *J. Power Sources*, **10** (1983) 219.
[17] L. R. Bacon, A. L. Sotier and A. A. Roth, *J. Milk Food Technol.* **16** (1953) 61.
[18] G. Sykes, *J. Appl. Bacteriol.* **33** (1970) 147.